2013

Study of composite wind turbine spars

Syed Shahrukh Zafar
Lehigh University

Study of composite wind turbine spars

by

Syed Shahrukh Zafar

A Thesis

Presented to the Graduate and Research Committee

of Lehigh University

in Candidacy for the Degree of

Master of Science

in

Mechanical Engineering

Lehigh University

May 2013

Certificate of Approval

This thesis is accepted and approved in partial fulfillment of the requirements for the Master of Science.

_____
Date

_____
Dr. Joachim L. Grenestedt

_____
Dr. Gary Harlow

Acknowledgements

The work presented in this report was carried out at the Composites Lab of the Department of Mechanical Engineering and Mechanics, Lehigh University between September 2011 and May 2013 under the supervision of Dr. Joachim L. Grenestedt. In addition to author, significant contributions to the project were made by Tianyi Luo, Prasad S. Naik, Jian LV, Robert S. Thodal, Jacob B. Patterson and William J. Maroun.

Help from Dr. Raymond A. Pearson of the Materials Science and Engineering Department at Lehigh University in resin formulation is greatly appreciated.

Table of Contents

1. List of Figures

2. List of Tables

3. ABSTRACT

This report presents a theoretical, numerical and experimental study of composite wind turbine spars under bending loads. Spars were made from commercially available glass/ carbon fiber material. The spars were composed of uniaxial (0°) flanges and biaxial (+/- 45°) shear webs. Items of particular study were co-block polymer additives in vinyl ester resins, a presumably new spar design, and using carbon fiber pultrusions for spar caps (flanges).

Composites are very strong and thus tend to be thin, which exacerbates the problem of buckling. Further, fibers also buckle at the micro level, leading to lower effective compression strength than tensile strength of a composite. Many structures tend to buckle in out of plane direction which can cause early and abrupt failure.

A 3-point bend test rig was manufactured in-house for experimentally testing composite spars. The experiments indicated abrupt failure without any sign or other form of damage. Limited number of spars was made with slightly different construction. All spars were subjected to same testing environment.

Finite element analyses were performed in order to shed light on the failure mechanisms leading to catastrophic failure. The FE code Ansys was used for the analyses. 3D models were developed, loads were applied, and linear elastic static as well as buckling analyses were performed. The results obtained from analysis were in reasonable agreement with the experimental tests.

4. INTRODUCTION

4.1. Background

With depleting and highly polluting conventional energy sources, many countries initiated and are moving towards clean and renewable energy, e.g. wind, solar, biofuel, biomass, tidal and hydro. Pragmatism and viability have outshined many other types of energy resources but hydro and wind. Concerns regarding power generation from water [25,26] motivated research and development of extraction of energy from wind. Great strides have been made with certain success in the sector of wind power. The key to the viability of extracting energy from wind through wind turbines is improvements in associated technologies and materials. In the past two decades, power output of wind turbines has grown from 250 kW to almost 8 MW and rotors have grown from 25m to over 125m in diameter. It is believed that for wind turbines to be commercialized and used as primary source of power generation, length of blades has to be increased but not at the cost of stiffness and strength [21,22,23]. UPWind has introduced an idea of upscaling of wind turbines in EWEA annual meeting in 2011 and claimed that a 20 MW wind turbine with rotor diameter of 175m~250m is feasible through innovative design [2].

The largest wind turbine today is E-126 by ENERCON with a rotor diameter of 126 m. It produces 7.58 MW of power. An 8 MW wind turbine by VESTAS is currently under production. The blade materials in most of these wind turbines are glass/ carbon hybrid infused with epoxy and balsa/ wood filling in shell core [1,15]. EWEA is committed to produce Europe's electricity by wind energy alone in a few decades [24].

The design of wind turbine blades is of critical importance in the overall performance of wind turbines because it is usually a trade-off between structural performance, aerodynamics, and cost [8]. The aerodynamics requires the blades to be long and thin but structural efficiency demands that the blade should be stiff, hence thicker or wider in particular at the root to bear large bending moment. Unfortunately, the thickness required to make the blade stiff and strong is greater than what is required for aerodynamic efficiency. Therefore a compromise is generally made between structural and aerodynamic efficiency. Quest for finding the best mix of both has brought many great aerodynamic and design innovations but comparatively slower improvements in material has rendered only a few choices in terms of materials to be used. Currently, composite materials play a significant role in the design of blades because of superior strength to weight ratios and comparatively higher resistance to weather [8,13,15,18]. The main composite material, glass fiber reinforced polymer, has withstood the test of time but carbon fiber although being expensive but lighter, in general stronger and approximately three times stiffer, may be a better choice. Because of the expense of carbon fiber, blades composed of glass / carbon hybrids may be preferable [10].

Large amounts of experiments conducted by DOE/ SANDIA/ MSU in USA regarding wind turbine blade materials, manufacturing and testing on continuous basis for years provide us an opportunity to make the best use of their findings and use manufacturing techniques based on their reports [6,7,10,13,15]. A vast variety of materials, its arrangements and testing procedures were implemented in these experiments. Materials such as glass fiber, carbon fiber and their combinations have extensively been used. As matrix epoxy, vinyl ester and polyester were used. For manufacturing, different versions

of liquid composite molding methods have been employed. As far as testing is concerned, most of the experiments are based on fatigue loading criteria, since it provides relatively realistic environment that blades are subjected to during operation.

4.2. Purpose of the present investigation

It is observed that in wind turbine blades there are both stiffness constraints (tip deflection, buckling) and strength constraints (static as well as fatigue) [14]. Blades are designed to withstand multiple types of loads i.e. aerodynamic, gravitational, centrifugal, gyroscopic and operational [21,22]. Aerodynamic loads produce lift forces that are dominant factor in every horizontal axis wind turbines and generate flapwise loadings.

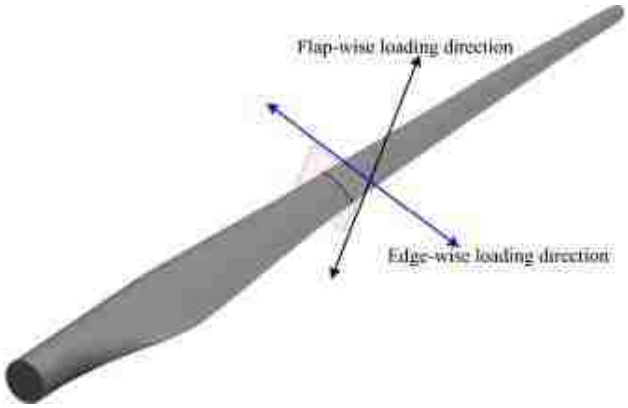

Figure 1: Wind turbine blade showing flapwise and edgewise loading directions

These flapwise loadings in turn produce bending loads along the length of the spar. It is of critical importance that these bending loads do not impart structural damage to the blades. Flapwise loading is mainly carried by a composite beam structure, or spar, inside the shell of the blade. A typical spar consists of spar caps or flanges, which carry axial loads and bending moments, and webs which carry shear and torsion. Fibers in the

flanges should run along the length of the blade because then they will be aligned with the highest stresses induced by axial and bending loads. As in any spar the flanges should be as far apart as possible, but this distance is limited by the shape of the blade. The flanges need to be connected with shear webs to transfer the load from one flange to the other. The shear loads are in general relatively low, so as far as strength is concerned the shear webs can be very thin. However, thin webs are prone to shear buckling [1].

Experiments for this report were designed to study strength, stiffness and failure mechanisms of spars under bending loads. A new form of co-block polymer was used in a vinyl ester matrix [20]. A presumably new spar construction was devised, where the spar was made in an inner and an outer half which were bonded together. Stiffeners were included to increase shear buckling strength. The two halves could be spaced to perfectly fill a cavity between pre-made blade skins. This would allow for a larger spacing of the flanges without risking that the resulting spar would not fit between blades skins. Today spars are often made unnecessarily small in order to guarantee that they will fit between the blade skins. The resulting gap is filled with a large amount of adhesive. This reduces structural efficiency (thinner spar), adds a lot of mass (adhesive), and creates a relatively brittle bond (thick adhesive). Finally, carbon fiber pultrusions were incorporated in the spar caps in a few of the spars.

5. LOAD CALCULATIONS

5.1. Spar for Wind Turbine

A spar will be designed for a wind turbine blade. However, a number of simplifications will be used. In particular, twist and out-of-plane loading will be disregarded. The design is thus similar to that of an airplane wing spar.

5.2. Spar Shear and Bending Moment

For an airplane wing, assuming a load factor n (e.g. n=3.8 or n=6) at limit load and a "safety factor" η (e.g. η=1.5 or η=1.725) and further that the lift distribution is constant along the span,

$$q = \frac{n\eta m_0 g}{b} \tag{1}$$

where m_0 is mass, g is gravitational acceleration and b is wing span, then the shear and bending moment in the wing are

$$\begin{aligned} T &= \frac{n\eta m_0 g}{2}\left(1-\frac{2y}{b}\right) \\ M &= -\frac{n\eta m_0 g b}{8}\left(1-\frac{2y}{b}\right)^2 \end{aligned} \tag{2}$$

if the width of the fuselage is neglected. The coordinate y is zero at the aircraft centerline and b/2 at the right wing tip.

At present the following parameters will be used:

m_0=250 kg

b=13 m

n=9

η=1.5

This leads to the limit loads

T_{max}=16554.4 N

M_{max}=53801.7 Nm

including a safety factor η=1.5 (for ultimate loads).

5.3. Buckling and Strength of Shear Webs

Assume Timoshenko's shear buckling formula,

$$\tau_{cr} = \frac{\pi^2 k_s E}{12(1-\nu^2)}\left(\frac{t}{b}\right)^2 \tag{3}$$

where for a long panel $k_s \approx 5$. The shear web will consist of three sections. The total height of the shear web is h (height of the spar), and the three sections will have the widths αh, $(1\text{-}2\alpha)h$, αh, respectively; see *Fig.2*. Here $0<\alpha<0.5$. The sections will have the thicknesses t, $2t$, t. The three sections will be subjected to the same shear loads per unit length N_{12}. Shear buckling in the first and third sections will occur when

$$N_{12} = \frac{\pi^2 k_s E}{12(1-\nu^2)}\frac{t^3}{(\alpha h)^2} \tag{4}$$

while shear buckling in the middle section will occur when

$$N_{12} = \frac{\pi^2 k_s E}{12(1-\nu^2)}\frac{(2t)^3}{\left((1-2\alpha)h\right)^2} \tag{5}$$

It is easy to show that minimizing the mass of the whole shear web requires shear buckling to occur simultaneously in the three sections, which leads to

$$\alpha = \frac{\sqrt{2}-1}{2} \approx 0.21 \tag{6}$$

If strength requires more thickness in the first and third sections, then their widths can be increased to reduce total mass (by reducing the width of the thicker middle section).

The shear loads per unit length in each shear web is approximately

$$N_{12} = \frac{T}{2h} \tag{7}$$

With E=20 GPa, ν=0.3 and h=90 mm, the minimum thickness is t=0.71 mm.

If the shear strength of the +/-45 degree glass fiber webs is 350 MPa, then the minimum thickness of the web is t=0.26 mm. Shear buckling can thus be assumed to be an active constraint, whereas shear strength is not.

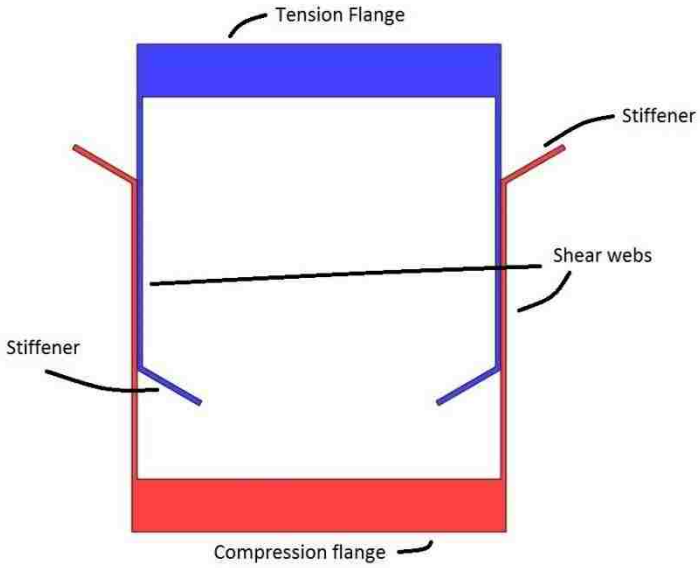

Figure 2: Cross section of spar

5.4. Spar Flanges

Assuming that the top and bottom flanges are thin with cross sectional areas A_f^{top} and A_f^{bot}, respectively, the flange stresses are

$$\begin{aligned} \sigma_f^{top} &= \frac{M}{A_f^{top} d} \\ \sigma_f^{bot} &= -\frac{M}{A_f^{bot} d} \end{aligned} \tag{8}$$

Note that the stress in for example the top flange depends linearly on the area of that flange, in spite of the fact that the neutral axis moves if only that flange's area is changed. Note also that the effective bending stiffness is

$$"EI" = E_f \frac{A_f^{top} A_f^{bot} d^2}{A_f^{top} + A_f^{bot}} \tag{9}$$

where E_f is the axial Young's modulus of the spar flange material. For a strength critical design, where the top flange is compression loaded and the bottom flange tension loaded,

$$\begin{aligned} \sigma_f^t &= -\sigma_{cr}^{comp} \\ \sigma_f^b &= \sigma_{cr}^{tens} \end{aligned} \tag{10}$$

and thus

$$\begin{aligned} A_f^{top} &= -\frac{M}{\sigma_{cr}^{comp} d} \\ A_f^{bot} &= -\frac{M}{\sigma_{cr}^{tens} d} \end{aligned} \tag{11}$$

where we used the definition that the compression strength is a positive number (e.g. σ_{cr}^{comp}=700 MPa, not σ_{cr}^{comp}=-700 MPa). For a unidirectional glass fiber reinforcement

with σ_{cr}^{comp}=700 MPa, the minimum area of the compression loaded flange would in the present case be A_f^{top}=854 mm^2. If the width of the flanges is 76.2 mm (3") then the thickness would have to be 11.2 mm.

5.5. Buckling of Compression Loaded Flange

The buckling load of a long uniaxially compressed simply supported rectangular plate is given by eq.12

$$N^{11} = -\frac{\pi^2}{b^2}\left(D^{1111} + 2D^{1122} + 4D^{1212} + D^{2222}\right) \tag{12}$$

if the width is b and if D^{1112}=D^{1222}=0. For an isotropic plate

$$\begin{aligned} D^{1111} &= D^{2222} = \frac{Eh^3}{12(1-\nu^2)} \\ D^{1122} &= \frac{E\nu h^3}{12(1-\nu^2)} \\ D^{1212} &= \frac{Gh^3}{12} \end{aligned} \tag{13}$$

resulting in

$$\begin{aligned} N^{11} &= -\frac{4\pi^2 Eh^3}{12(1-\nu^2)b^2} \\ \sigma &= -\frac{4\pi^2 Eh^2}{12(1-\nu^2)b^2} \end{aligned} \tag{14}$$

The present spar flanges are neither isotropic nor homogeneous. However, if they were and if E=20 GPa, ν=0.3, b=76.2 mm, h=10 mm then σ_{cr}=1.2 GPa which is well above the compression strength. It appears reasonable to assume that for the present case

compression buckling of the compression loaded flange will not occur before material compression failure [11].

5.6. Load Introduction

A three-point bend specimen of half the span would have the same maximum shear force and bending moment. The force on the central support would be

$P=2T_{\max}=33108.8$ N

If this were carried by a pin of diameter $D=25.4$ mm and the material thickness of the web were $t_p=4$ mm then the bearing pressure would be

$$p = \frac{P}{2Dt_p} = 217\,\mathrm{MPa} \tag{15}$$

6. MANUFACTURING

Established liquid composites molding manufacturing techniques as used for Navy ships as well as by DOE/ SANDIA/ MSU for wind turbine spars were employed in the making of the present spars. One of the standard techniques of manufacturing is to make a box spar [1,6,7,10,13,15]. It was decided to make the box spar in two separate halves, i.e. an inner half and an outer half and join them together with an adhesive. A total of seven spars were made and tested. Test was carried out after construction of each spar; hence it provided an opportunity to implement better manufacturing technique than the previous one. Each successive spar was built with slight variation and improved technique.

6.1. Materials

The outer spar halves were built on the outside of a 76.2 mm x 76.2 mm x 6000 mm aluminum extrusion with an HDPE routed piece installed on the bottom to make the stiffener as can be seen in *Fig.3*. Inner spar halves were built inside a 76.2 mm x 76.2 mm x 6000 mm aluminum extrusion of which top surface material had been milled out, and two HDPE routed pieces installed on the web as shown in *Fig.4*.

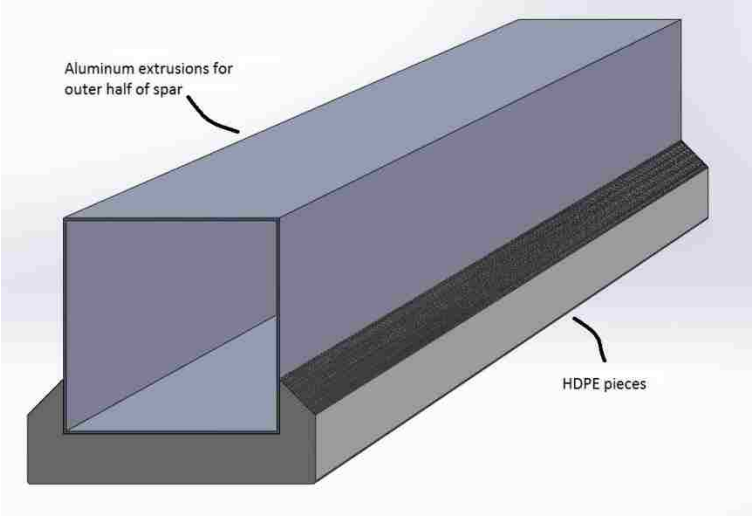

Figure 3: Aluminum extrusion and HDPE piece for outer half of spar

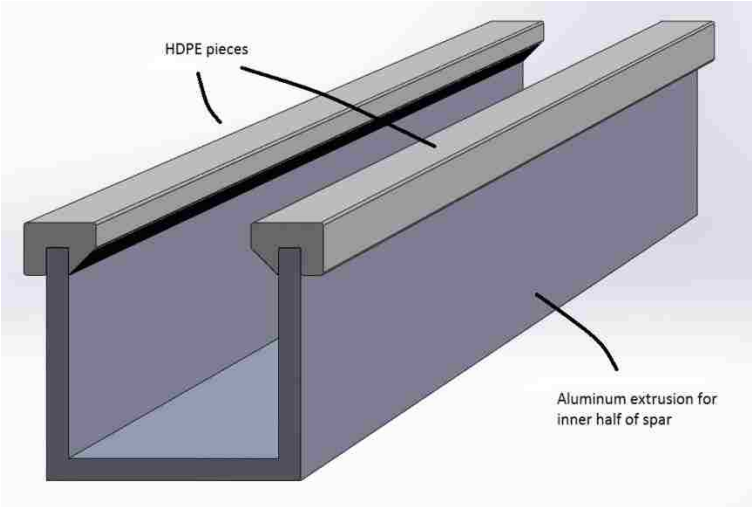

Figure 4: Aluminum extrusion and HDPE pieces for inner half of spar

Essentially uniaxial (0°) fibers were used for the flanges to bear bending loads and biaxial (+/-45°) fibers were used for the shear webs. Woven Owens Corning A260-50 (uniaxial) and DB240 (biaxial) were used for subject experiments. Solid flat carbon fiber pultrusions with dimensions 11 mm x 1.76 mm were also used in some spars to reinforce the flanges. Material of peel-ply was nylon.

To make a bond between the two spar halves, Pro-Set ADV 176 was used with hardener Pro-Set ADV-276. The same aluminum extrusions and HDPE routed molds were used in the making of all spars.

6.2. Spar manufacturing process

6.2.1. Aluminum extrusion preparation

Both halves shared similar layup arrangement. The process started with cleaning and polishing of aluminum extrusions. 3~5 coats of release agent NC-770 was applied to the active surfaces of these extrusions and HDPE pieces so that infused spar could be taken out easily after cure. Routed HDPE pieces were installed appropriately on the inner and outer halves as shown in *Fig.3 and 4.*

6.2.2. Layup and arrangement

a. One layer of DB240 (+/-45°) running along the whole length of the beam was laid directly on the mold for webs and flange as shown in *Fig.5.*

Figure 5: Layer of DB240(+/-45°) on aluminum extrusion for inner half

b. One layer of A260 UNI glassfiber, as shown in *Fig.6*. This was folded forward and back to make the flange. In the center the UNI glassfiber was 15 plies thick.

c. One layer of DB240 (+/-45°) transverse to the beam, covering webs and flange. It took 4 pieces to cover the length of the spar. Overlap of at least 30 mm was set.

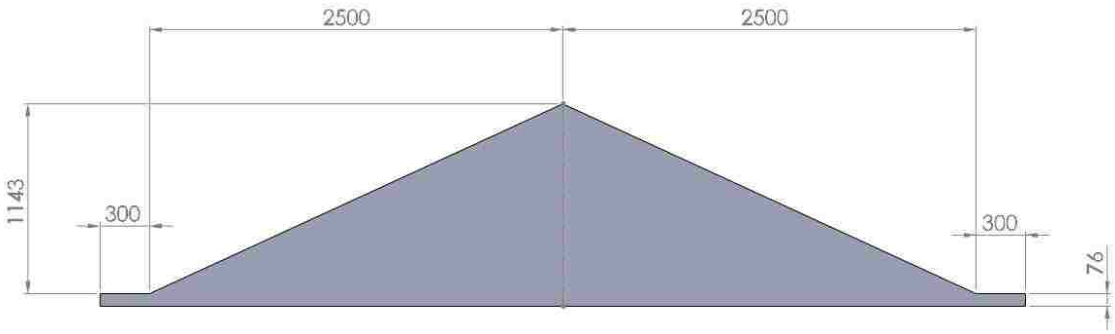

Figure 6: Shape of Uni layer in mm

d. Six layers of DB240 (+/-45°) reinforcements in the center covering both webs and the flange were laid to supposedly provide extra strength needed to counter buckling and stress concentration due to the holes needed for pinned end support. Lengths were 350 mm, 300 mm, 250 mm, 200 mm, 150 mm and 100 mm.

e. Three layers of DB240 reinforcements (+/-45°) centered at +/- 2500 mm from the center covering both webs and the flange were also laid due to same above stated reason. Lengths were 200 mm, 150 mm and 100 mm.

f. One layer of peel-ply was laid on the whole length of the beam covering both webs and the flange. Extra width of peel-ply material was used to make it easier to manage corners and wrinkles while vacuuming. Peel-ply impregnated with release agent helps in easy separation of laminate and vacuum bag after infusion as shown in *Fig.7*.

g. A perforated distribution medium covering flange only was laid on top of peel-ply as shown in *Fig.7*. Spiral pipes were placed in the middle of the distribution medium that ran along the length of the spar to assist in resin transfer during the infusion process. Spiral pipes were placed almost 1" higher from the surface to prevent any contact with the spar.

h. One breather cloth folded into three layers was taped underneath the beam in order to provide a continuous passage for the air inside the bag while vacuuming.

i. The aluminum extrusion along with laminates were then put inside a vacuum bag and sealed at both ends with bag sealant tape as seen in *Fig.8*.

j. A small hole was made in the bag on one side of aluminum extrusion at the bottom and a vacuum pump pipe was connected to the breather with help of sealant.

Figure 7: Peel Ply and distribution medium on aluminum extrusion for outer half

Figure 8: Vacuum bag covering aluminum extrusion of inner half

6.2.3. Vacuum process

Vacuum was created with the help of a pipe connected with breather at one end and a pump and pressure gauge at the other. It was desired that the vacuum pressure was maintained near 100% so that it can be ensured that there is no air trapped inside the bag and infusion process could take place as efficiently as possible. While vacuuming, effort was to make sure that corners of the laminates remain sharp so that accumulation of resin could be avoided. The spars were kept under vacuum overnight for compactness and removal of air.

6.2.4. Infusion

Infusion of the spar was performed after making sure that the system was vacuum tight. A process called vacuum assisted resin transfer molding (VARTM) was used for infusion. It was calculated that to cover all parts of the spar, around 6 liters of resin would be required. A proper mix of the chemicals was made as shown in *Table.1*.

The mix was then stirred thoroughly and put in a vacuum container for degasification for about 20 min. After removal of majority of bubbles, resin was sucked into the vacuum

Chemicals	Quantity
Resin *(DERAKANE® 8084)* [27] (Spar 1 only)	6 liters
Resin (*EPOVIA® RF1001L-00)* [28] (Spar 2-7)	6 liters
Luperox® IS300 [28]	1.25% of resin by weight
Methyl Ethyl Ketone Peroxide (MEKP)	1.25% of resin by weight
Cobalt Naphthenate (CoNap, 12% concentration)	0.15% of resin by weight
Inhibitor Solution (12% HQ)	0.07% of resin by weight

Table 1: Chemicals used in infusion

bag via pipes on one end, running through the length of the spar. It took around 20~30 minutes for the resin to reach the other end. Pipes were folded to stop the supply of resin once resin reached all the parts of the spar but vacuum pipes were kept open until resin was cured. The spar was then covered with insulated housing and heated up to 70 $^{\circ}$C with the help of heating strips. The heat started the curing of the resin. Inner and outer halves were manufactured and infused with the same technique.

6.2.5. Adhesive bonding and post cure

Initial curing was done for at least 12 hours. The spar was then taken out of the vacuum bag and the HDPE pieces were removed. The edges of the spar were trimmed off for safety purpose.

Once the inner and outer halves were made, they were joined together with epoxy resin Pro-Set Adhesive 176 [29] mixed with Pro-Set ADV-276 hardener [30]. The distance between the two halves was maintained by an 80 mm spacer. The shear webs of the two spar halves were adhesively bonded. Blind (pop) rivets were used to apply bonding pressure and to index the two halves relative to each other. The adhesive cured under room temperature. The spar was then post cured at 90°C in a specially designed oven (with light bulbs as the source of heat). After post heat treatment, holes for pinned end supports were drilled with vertical drill machine at both ends, 2.5 m away from center of spar. The spars were then installed on a 3 point bend test assembly (refer Testing section) and were subjected to bending loads.

6.3. Modifications

Following necessary variations and modifications were performed on successive spars after each test.

a. New resin, *EPOVIA® RF1001L-B1 [28]* was purchased and used after the testing of first spar. It has been suggested in [17] that a good fiber/ matrix interface can improve compression strength as well as compression modulus.

b. After first test, Luperox IS-300 was added with resin appropriately [refer *Table.1*] to make infusion stable for long periods at ambient or slightly higher temperatures [28].

c. In six of the seven spars that were manufactured, rivets were used in order to get a more uniform bond line and in order to index the two spar halves relative to each other.

d. When fibers were cut along the length of fiber roll for flanges, it was ensured that every strand is separated neatly and no fiber gets damaged.

e. First five tests resulted in premature failure of spar, possibly by failure in the compression loaded flange, possibly by shear buckling of the webs, or possibly even by adhesive failure in the joint of the webs. It appeared that the web thickness required to prevent buckling may not have been sufficient. With the intention of strengthening the spar against buckling, web thickness of the last two spars was increased with additional layers of glass fibers having symmetric layup.

f. Carbon pultrusions were added in the flange section with the intention to provide additional strength, and in particular stiffness, against flapwise bending loads in three spars as shown in *Fig.9*.

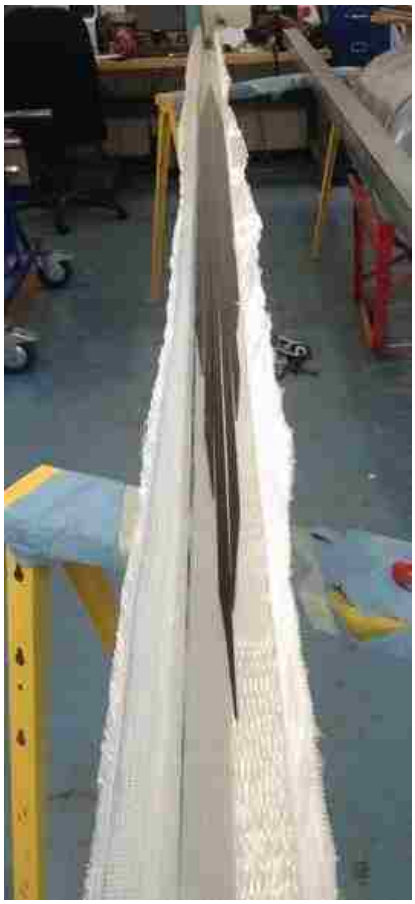

Figure 9: Layup of carbon fiber pultrusions on flange for inner half

6.4. Difficulties

Several difficulties were faced during construction of the spars.

a. Since it was a hand layup process, despite best efforts small kinks in the fibers may have been present. These flaws under compressive loads may have resulted in micro-buckling, which may ultimately have resulted in the failure of the spar [3,4,5,7].

b. While vacuuming the inner half, it was difficult to maintain sharp corners. Sharp corners are desired because if there remains a cavity beneath the corners, that space is filled by resin without laminate reinforcements, which are potentially low strength areas and may contribute to early failure of the structure.

c. Possible presence of small gaps in between bag sealant tape and aluminum extrusion may have resulted in entrapment of air bubbles while vacuuming which may have resulted in voids and gaps in the matrix.

d. It was difficult to ensure smooth surface finish of active surfaces of HDPE pieces because same molds were used for all spars and removal of resin from these surfaces after each spar construction, gradually deteriorated them.

e. Lead hammer was used to put the molds in place and also to remove them from aluminum extrusion. This hammering produced permanent bend in the molds and it became difficult to install them in last few spar constructions.

f. Taking out spar from aluminum extrusion became difficult because the heat applied to cure the resin also expanded spar inside the aluminum extrusion. Considerable force was required to take the spar out of the extrusion. Since force was applied at one end while the rest of the spar was still inside the extrusion, it produced bend.

g. Heat was provided to cure the liquid resin. Peel ply and distribution medium (which were just above the laminates) stuck to the resin during solidification. It was difficult to take them out of the spar without any deterioration of spar surface.

7. TESTING

7.1. Test Setup

All the spars were tested statically on an in-house fabricated 3-point bend assembly [*Fig.10*]. The main objective of these tests was to identify the maximum load spars can carry before they fail and its comparison to the design load. A total of seven spars were manufactured and tested.

Since spars were tested in bending, same compressive and tensile forces were induced in the fibers. The test was setup so that each spar was loaded in a flapwise direction on the test assembly in a way that the inner half was facing upwards and carried tensile loads. The outer half, facing downwards at the bottom carried compression loads. The spar was mechanically fastened via 4130 Chromoly pins of diameter 25.4 mm to the fixed pinned end supports on both sides which were 5 meters apart. The center of the spar was also fastened to 4130 Chromoly pin of diameter 25.4 mm.

7.2. Loads and sensors

The center bearing support was pulled upwards through a load cell for electronically sensoring load values by a remote control operated winch with a lifting capacity of 53000 N. A pictorial representation can be seen in *Fig.10.*

A string gauge was mounted just beneath the center of the spar for registering center deflection. Spars were loaded and unloaded in a stepwise manner.

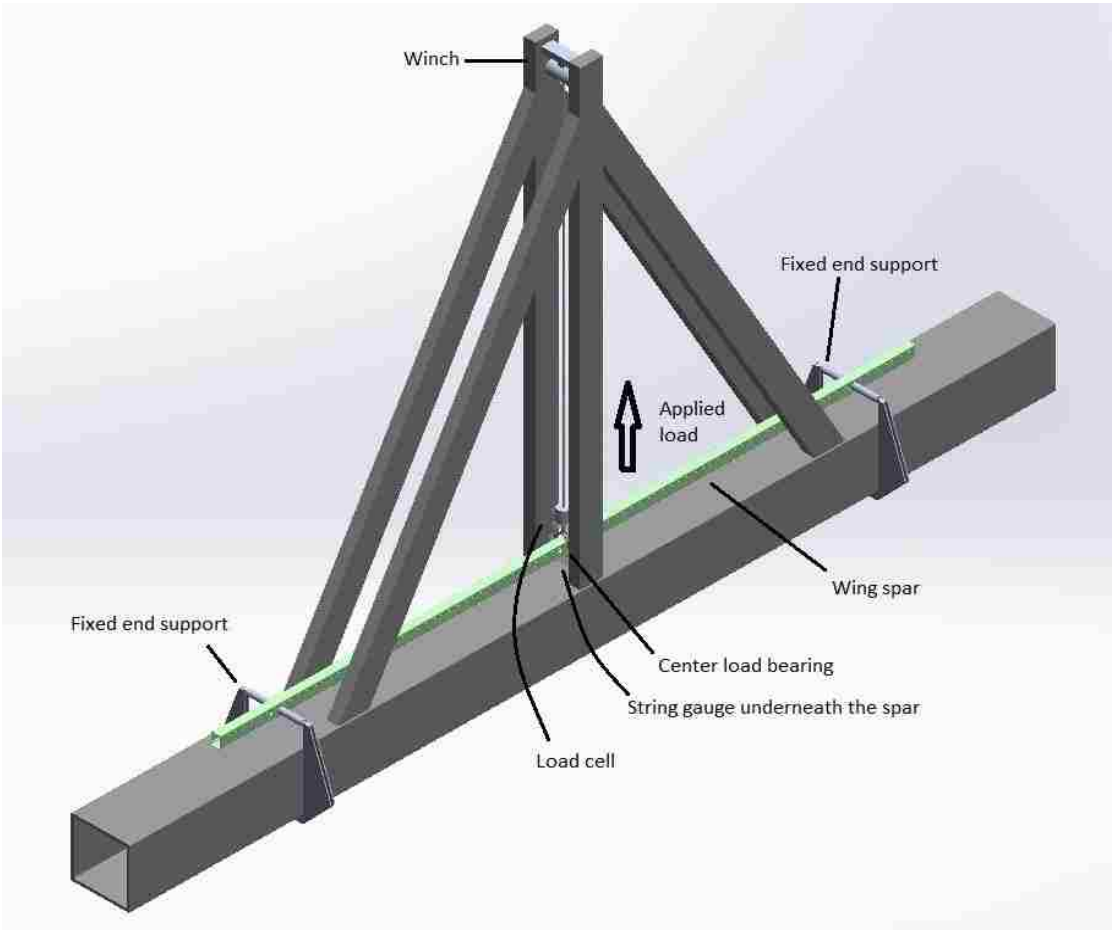

Figure 10: 3-point Bend Assembly

7.3. Common failure mechanisms

The spars were made of multidirectional composites with varying volume of fiber content. Following studied and established failure criterions in composite structures give us an opportunity to investigate our results within acceptable limits and can be referred in [19].

a. Failure is generally progressive and occurs from the gradual accumulation and interaction of dispersed damage, rather than initiation and growth of a dominant crack.

b. As damage accumulates, the constitutive relations of the material may change significantly.

c. Several damage modes can be identified such as fiber dominated tension and compression, matrix dominated cracking parallel to fibers, and inter-laminar cracking between plies. Some of these modes can produce failure directly, such as fiber dominated modes while modes like matrix cracking may have an indirect effect on failure by causing load transfer onto fibers.

d. Under tensile loading, the strains to produce matrix cracking in off-axis plies are generally well below those to produce fiber failure. As a consequence, in multidirectional composites, cracking tends to initiate first in plies where the fibers are at the greatest orientation relative to the maximum tensile stress. Cracking accumulates in these domains (90° plies), followed by domains of lesser orientation (45° plies).

e. Delamination between plies may also occur at cut edges, free edges, ply terminations, or at intersection of matrix cracks in adjoining plies. Gross failure often occurs by fiber breakage in any domains oriented nearly parallel to the maximum stress (such as 0° plies). Under compressive loading the strains to produce matrix cracking in off-axis domains are often comparable to those for fiber dominated failure, so damage development in a matrix dominated mode may also produce gross failure.

f. Performance of a composite structure in general heavily depends on the material systems used, particularly the type of fiber and style of reinforcement (parallel aligned layers, woven, chopped).

g. Kinks and waviness in the fiber may give rise to micro buckling which may adversely affect the strength of composite structure under compressive loading.

h. Early delamination due to stress concentration at ply drops and ply joints may occur.

i. Hot/wet conditions may act as a catalyst to failures of composites.

j. Debonding of joints is a major constituent in composite failures which may occur due to surface preparation deficiencies, voids, porosities, thickness variations in the bond layer, etc.

7.4. Observed failure mechanisms

It is important to observe and study actual failure mechanisms so that better design parameters can be developed and incorporated in future spar structures to obtain ideal results. Observation of failures was done by visual inspection. Failures can be categorized into following types.

7.5. Types of observed failures and explanation

As mentioned above, only visual inspection of the failures was performed. Many different modes of damages could be seen on a single spar. They can be categorized as follows:

7.5.1. Buckling in shear webs

Of the seven spars that were tested, most failed early on the application of load and ultimately produced buckling in shear webs [*Fig.11and12*]. Damages incurred on spars after the application of load may have forced webs to deflect in out of plane direction. Since the two halves were connected through shear webs, it seemed that first five spars with thin webs construction could not sustain the stresses induced due to bending and failed at loads much lower than design load. Furthermore, it was noted from earlier research that if multiple layers are added together with each layer oriented in various preferred directions, material will become preferentially strong in that direction. Hence shear webs in last two spars were reinforced with additional layers of glass fiber (+/-45°, symmetric) in an attempt to avoid buckling failure.

Figure 11: Buckling in webs and deformed compression flange

Figure 12: Debonded webs

7.5.2. Damage formation/ growth in the adhesive layer between shear webs

All spars suffered from severe damage in the adhesive layer bonding between shear webs. These adhesive failures may have led to the final failure of the spar, or they may have occurred for example after shear buckling of the webs. Theses failures can be further categorized as cohesive shear failure and adhesive shear failure [16]. Damage in adhesive layer was observed at different places in all spars.

Figure 13: Debonding of shear webs

7.5.3. Effects of stress concentration around holes

Adhesive-riveted joints were used except in first spar which may have resulted in extra strength between webs of inner and outer halves under bending. Cracks were seen around rivet/ pin holes which may have been produced or propagated due to stress concentration. Also, use carbon fiber pultrusions with untreated surface may create serious potential of stress concentration [9].

Figure 14: Crack passing through rivet hole

7.5.4. Internal damage formation/ growth in laminates/ plies

The flanges were subjected to tension and compression. Severe damage in terms of delamination was observed after final failure. The delaminations may have occurred directly after the final failure. Delamination and debonding of plies in shear webs were also observed especially near rivet holes.

Figure 15: Delamination of plies in shear webs & compression flange

7.5.5. Splitting and fracture of fibers

Splitting and fracture of fibers were seen at many places on the spar after the experiment. On tension flange, fiber fracture could be seen at several places. Compression flange mostly consisted of delaminated skins along with fiber fracture. Delamination and severe fiber fractures were observed in the shear webs of both halves which may have resulted because of buckling. Severe delamination and splitting at the corners were also observed.

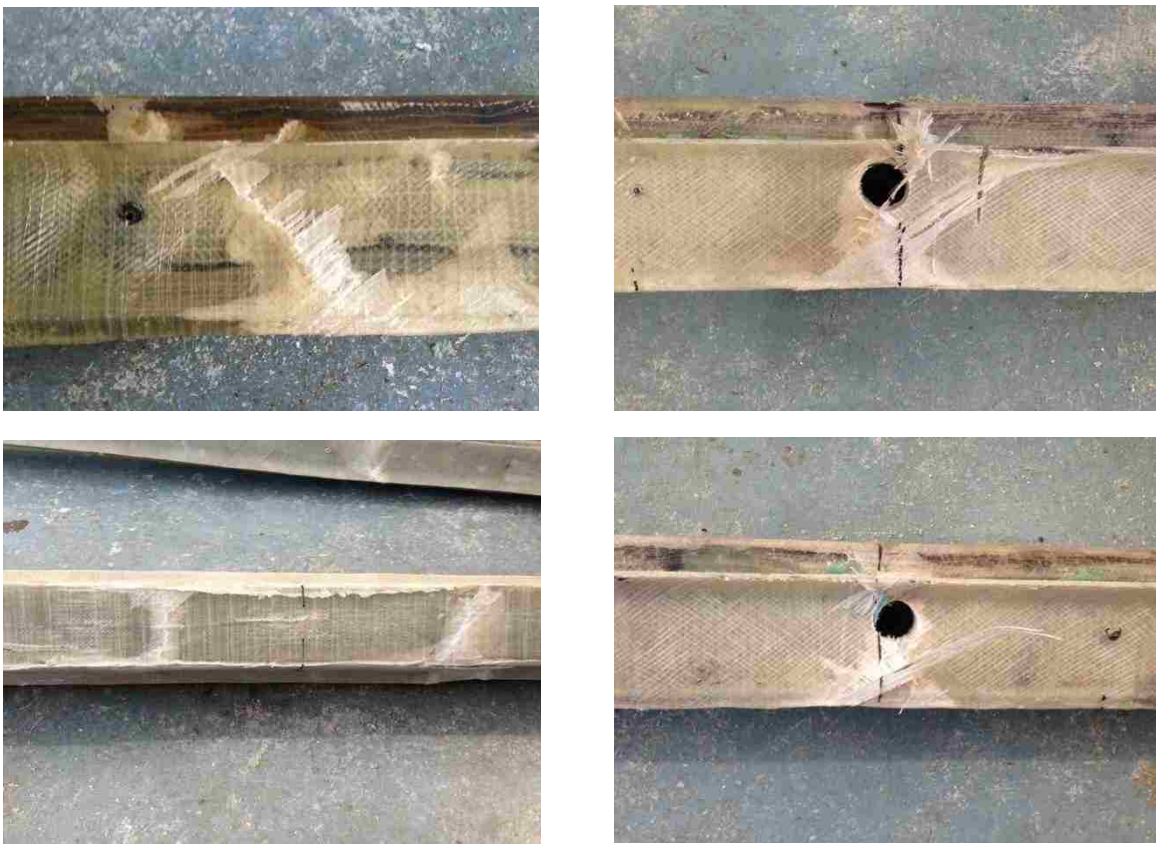

Figure 16: Fiber failure and splitting at various locations along spar

7.5.6. Miscellaneous

Since the flanges of the spar contained multiple layers of glass fiber one over another, the existence of ply drops may have contributed to high inter-laminar stresses and may have contributed to delamination on the compression side under bending. It is noted from previous works that ply drop pinking or chamfering may be an effective method to reduce this kind of damage [6].

Another interesting fact observed after the experiments were that signs of fiber failure was not only localized at the region of ultimate failure but were dispersed all across the spar. This may be due to the dynamic (almost explosive) failure of the spars. Recall that the spars were designed to fail essentially everywhere at the same load.

Strength in a spar may vary from place to place and ultimate failure is supposed to originate at the weakest spot or at the largest flaw.

7.6. Recorded data

As mentioned earlier, load cell and string gauge were installed to record applied loads and subsequent center displacement of the spar. Results obtained from testing of 7 spars are presented in *Fig.17* to *Fig.23* below. The first line of caption describes the type of reinforcements in both halves of spar and the second line shows additional reinforcements in shear webs.

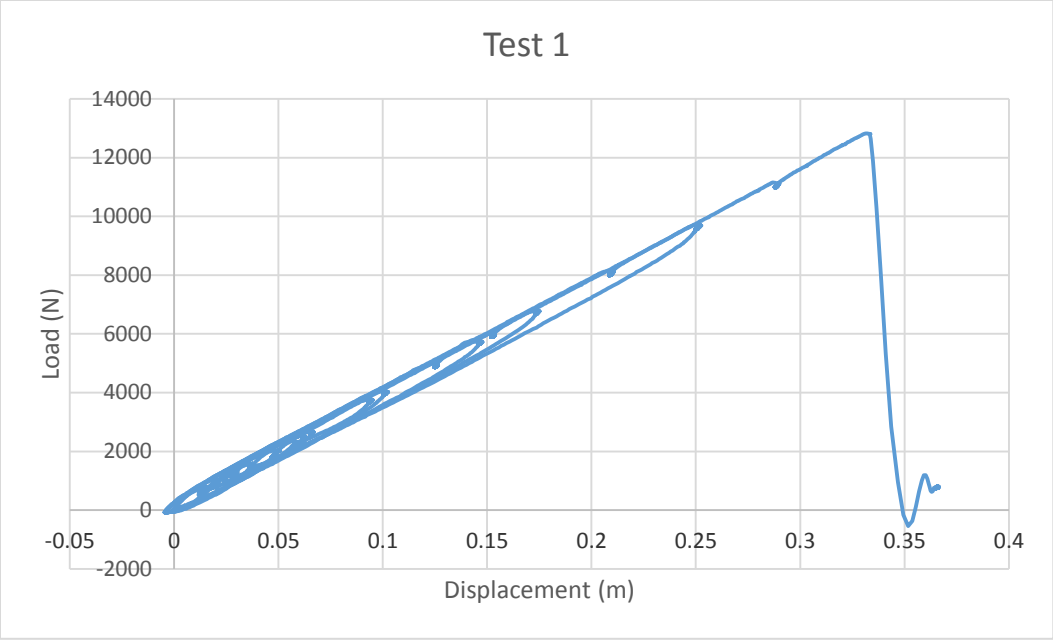

Figure 17: both halves glass fiber reinforced

both halves with thin webs

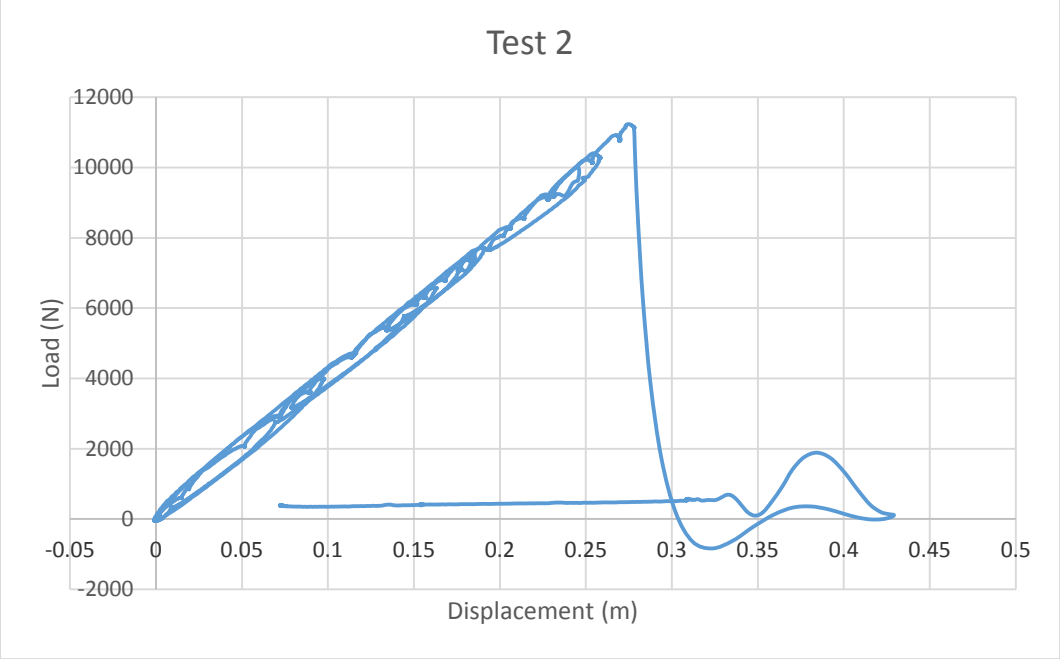

Figure 18: both halves glass fiber reinforced

both halves with thin webs

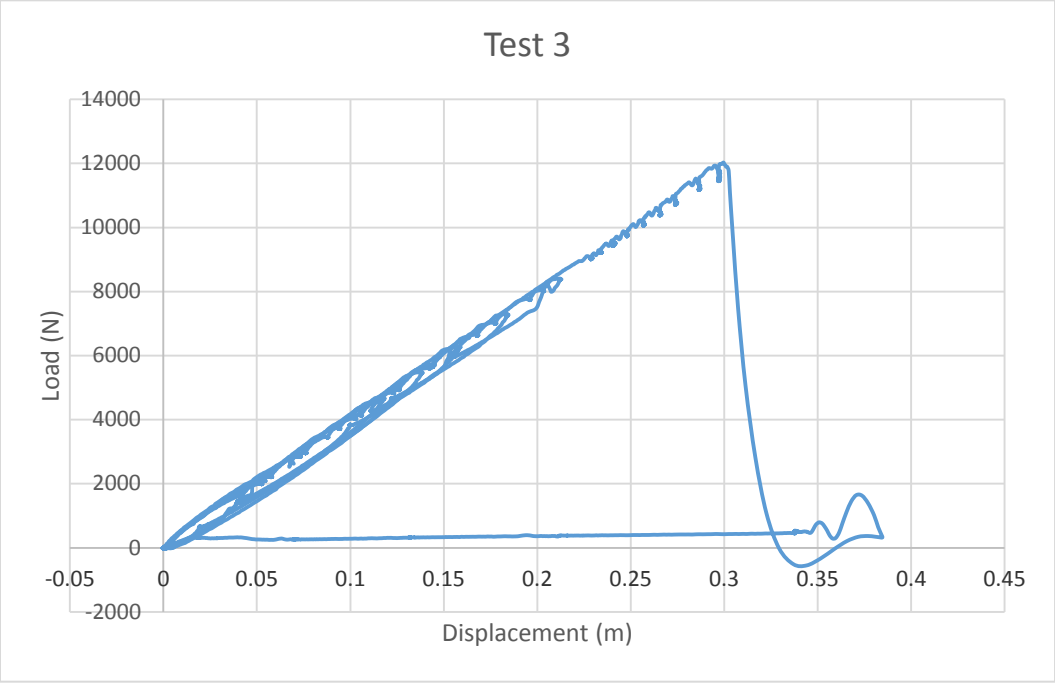

Figure 19: both halves glass fiber reinforced

both halves with thin webs

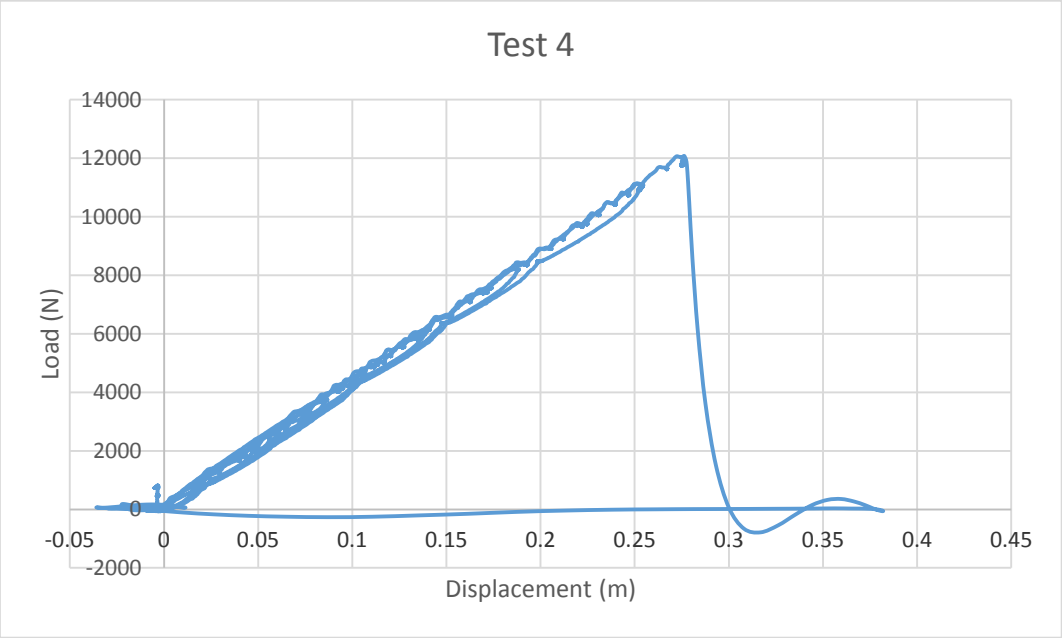

Figure 20: both halves glass fiber reinforced

both halves with thin webs

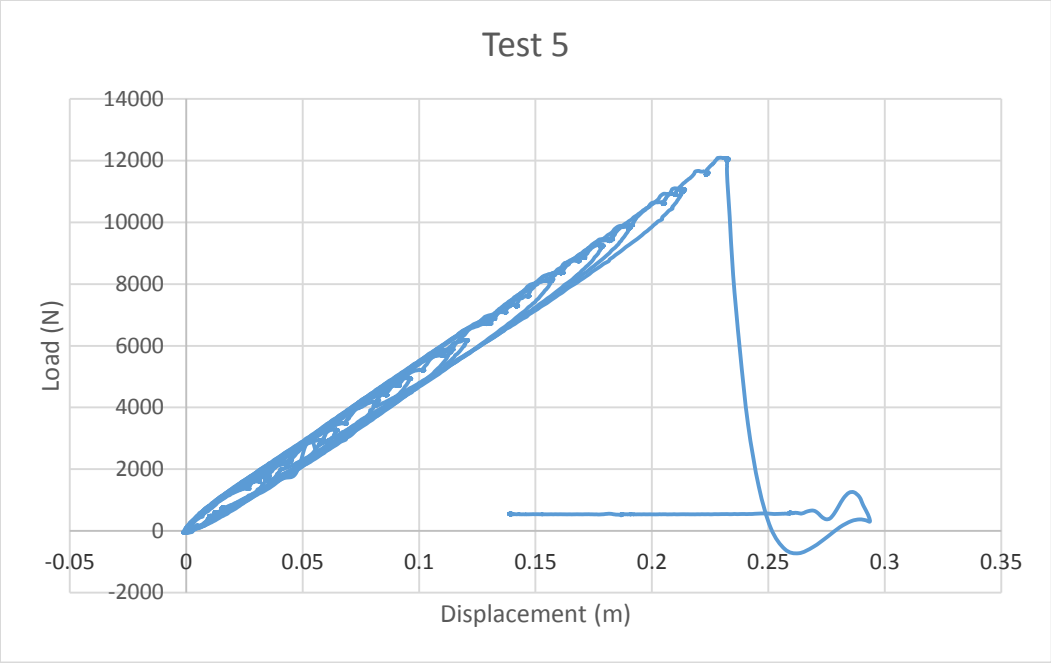

Figure 21: only inner half flange carbon fiber reinforced

both halves with thin webs

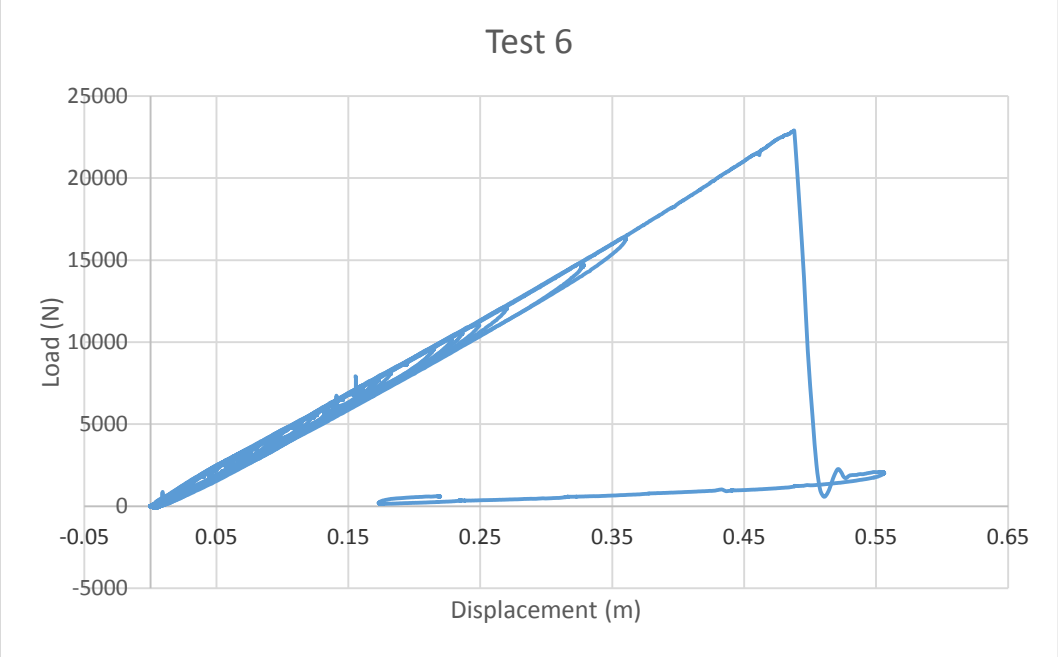

Figure 22: both halves glass fiber reinforced

both halves with thicker webs

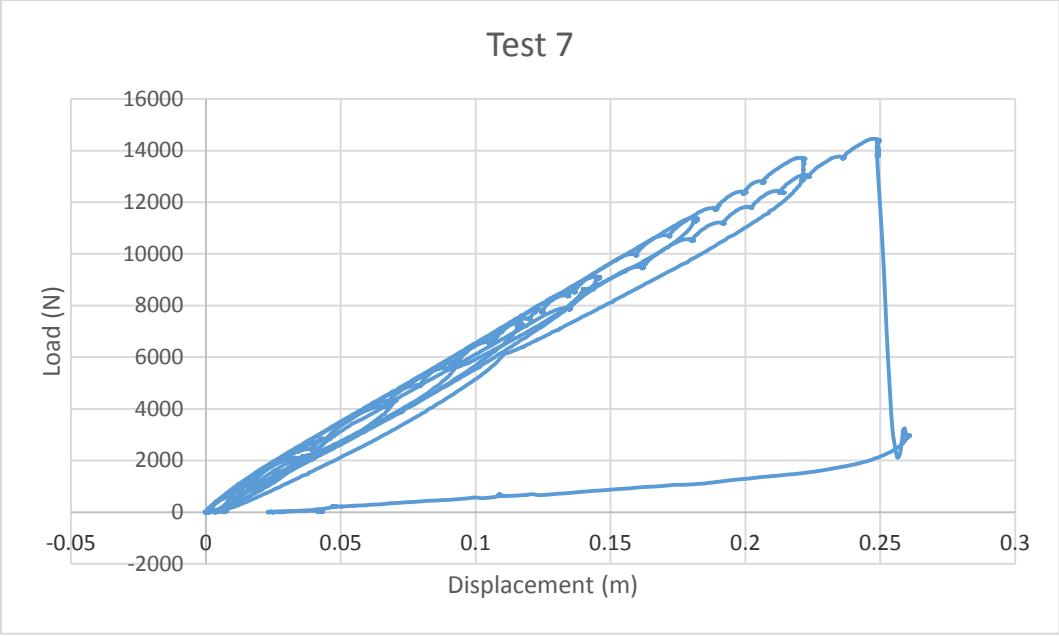

Figure 23: both halves carbon fiber reinforced

both halves with reinforced webs

7.7. Summary

Above charts represents the amount of center deflection of spars with respective stepwise load increments. Sixth spar test exhibited the most optimum result as it took load that was closest to design load before failure. It may be inferred from empirical results that additional reinforcement of shear webs may have played a very critical role against buckling, although it cannot be said with confidence that the failure of sixth spar was due to compression or shear. Moreover, use of carbon fiber pultrusion in the flanges of fifth and seventh spar may have contributed in additional strength and stiffness but full potential of carbon fiber reinforcements could not be tested since these spars failed earlier than design load limit.

Same experiment was then modeled and analyzed in Ansys, results of which are described in next chapter.

8. FINITE ELEMENT ANALYSIS

8.1. Problem definition

As described in introduction, spar is usually the main load carrying structure in wind turbine blades. They carry flapwise loading and in turn are subjected to bending. It has been noted from earlier experiments that bending may produce buckling in shear webs which can cause early failure. Hence it is critical to optimize thickness of flanges and shear webs so that they may be able to resist buckling but are aerodynamically efficient as well. Finite element technique was used to study the spars. The objective was to obtain general behavior of spar with specific materials/ orientations under bending loads.

8.2. Modeling

3D spar modeling and simulations were performed in FE code Ansys. Symmetry of spars was used to ease the complications and time required for the analysis. Observations from experiments suggested that the thickness of shear webs might have played a critical role in resisting buckling failure in the spar. Hence two models were made, one with thin webs and another with reinforced (thick) webs. Static analysis of model with reinforced webs was performed and both models i.e. thin & reinforced webs were subjected to buckling analysis. Buckling analysis results were generated for spar with thin and reinforced webs separately and then compared.

Following is systematic representation of procedures used in code writing:

a. *Beam* was defined as *element type*

b. *Shell91* was used to construct non-linear thick layers.

c. *Keypoints* were defined on the corners and along the geometry

d. *Lines* were created between *keypoints*

e. *Triangular areas* were made

f. *Degree of freedom* was defined for the layers

g. Flanges and webs were plied with *0° A260 & +/-45° DB240* layers

h. *Anisotropic* properties were defined

i. *Orientation* for *0°* and *45°* layers were defined

j. All lines and areas were *attached* to each other

k. Structure was *meshed*

l. *Boundary conditions* were applied

m. *Load* was applied to the structure

n. *Solution* was generated

8.3. Static Analysis

Linear elastic static analyses are represented by *Fig. 24, 25, 26 and 27.* Model was setup such that one end of the structure was fixed in y and z translation and x and y rotations and load was applied on the other end with fixed translations in x and z and fixed rotations in x and y. As mentioned earlier, symmetry condition was used in results extraction to minimize computational time and load required to analyze the results. Maximum displacement on the application of design load can be observed in *Fig.24.*

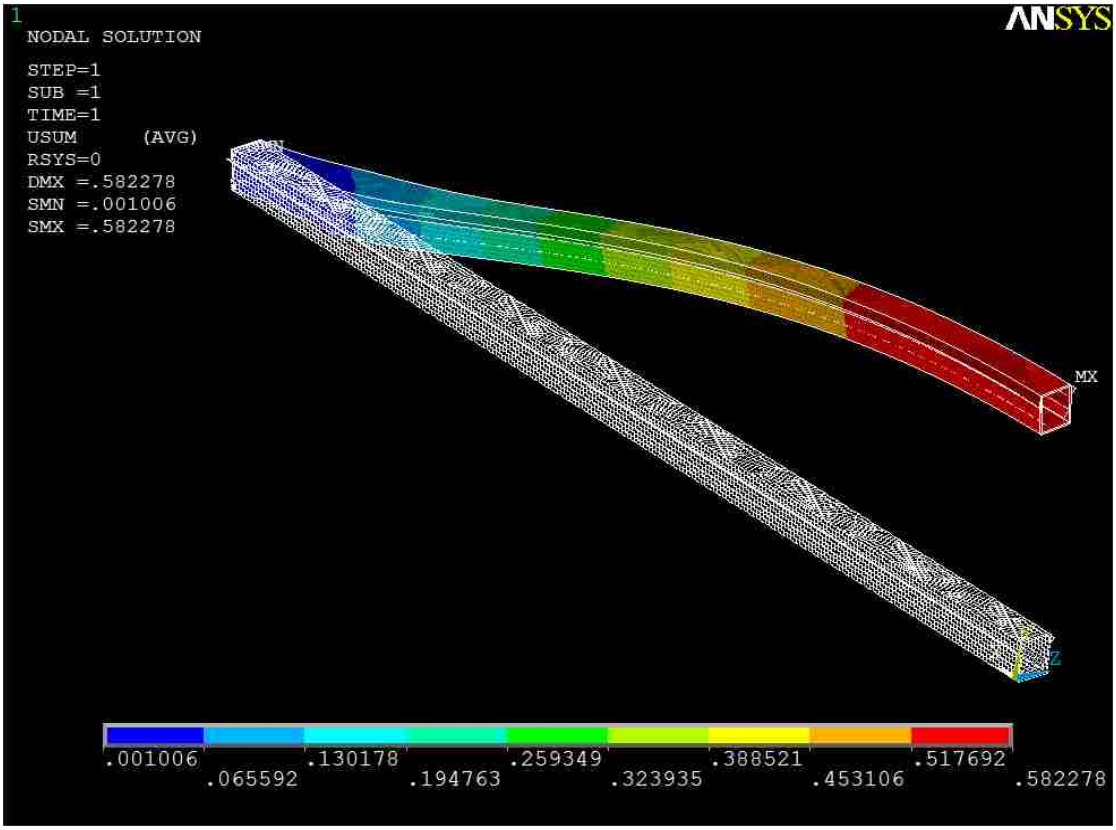

Figure 24: Static displacement (in meters) of spar at full load

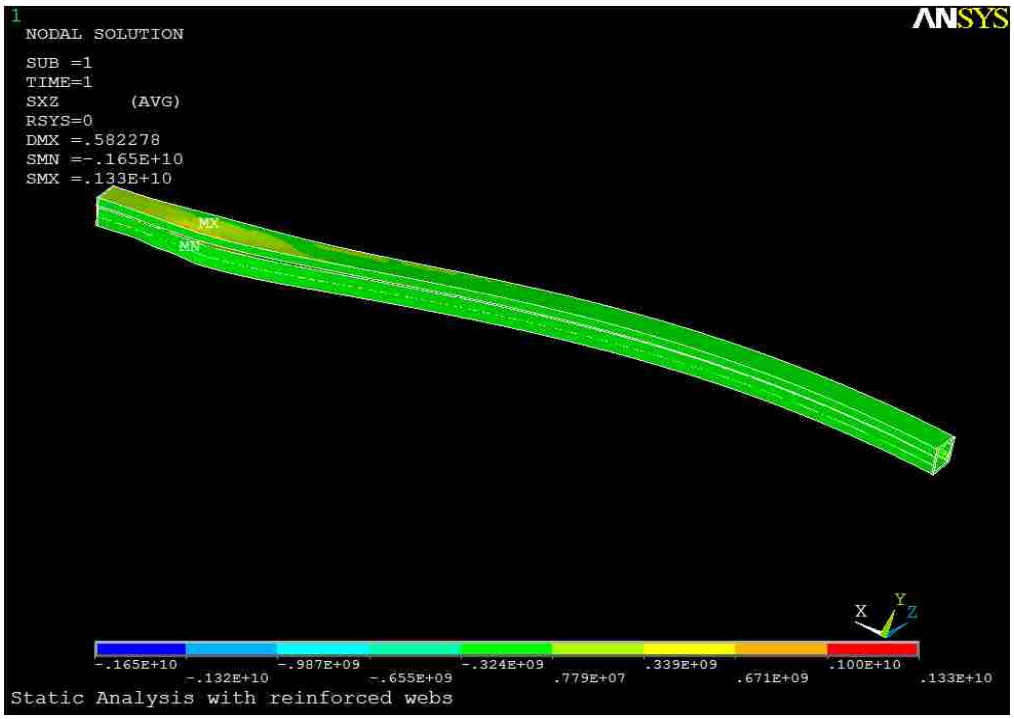

Figure 25: Shear stresses in xz-plane at maximum displacement

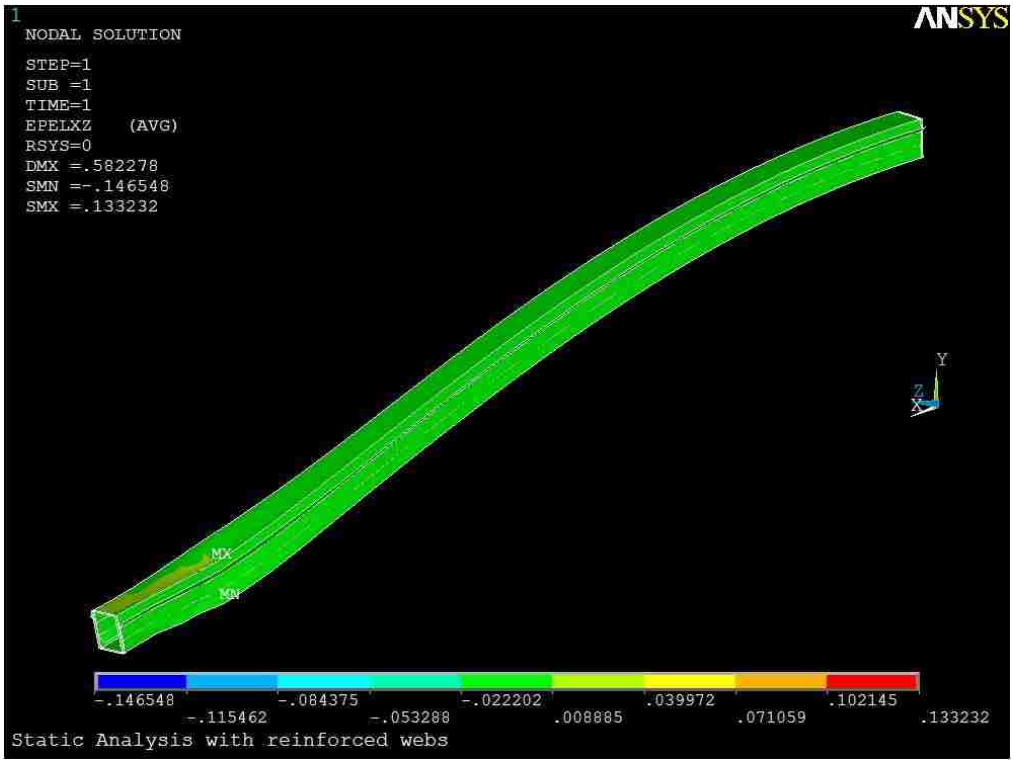

Figure 26: Strains in xz-plane at maximum displacement

8.3.1. Summary

It can be observed from *Fig.24* above from static analysis that deflection in spar on the application of full load i.e. 33000 lbs. [refer Load calculations] is approximately 600 mm which is close to what we observed from *test 6 [refer Testing]*. Shear stresses and strains in xz-plane (i.e. along and across the direction of uniaxial fibers) in *Fig.25 and 26* suggest that shear load in web is above the buckling load calculated before in Load calculation section. In bending, load is transferred between flanges via shear webs. That is why flanges incorporate some biaxial plies to transfer load to shear webs efficiently. Since maximum stresses and strains are apparently induced in webs, it seemed webs needed additional reinforcements to effectively carry the transferred loads.

Analysis showed maximum stress and maximum strain in shear webs rather than flanges which indicate that spar may fail in buckling. Thus buckling analysis became necessary to find the effective failure modes in the spar.

8.4. Buckling Analysis

Spars models with thin and reinforced webs were subjected to *eigenvalue buckling analysis* as shown in *Fig.27~30*. Models were loaded with same amount of force as in static analysis and same boundary conditions were applied. Objective was to analyze results where eigenvalue is closest to 1. Results obtained indicated that buckling strength was approximately one-third in the spars with thin webs.

Buckling may still have been the dominant failure mode in both cases i.e. with thin webs [*Fig.27* and *Fig.28]* and also with thick webs [*Fig.29* and *Fig.30]* but with much reduced effect in the later.

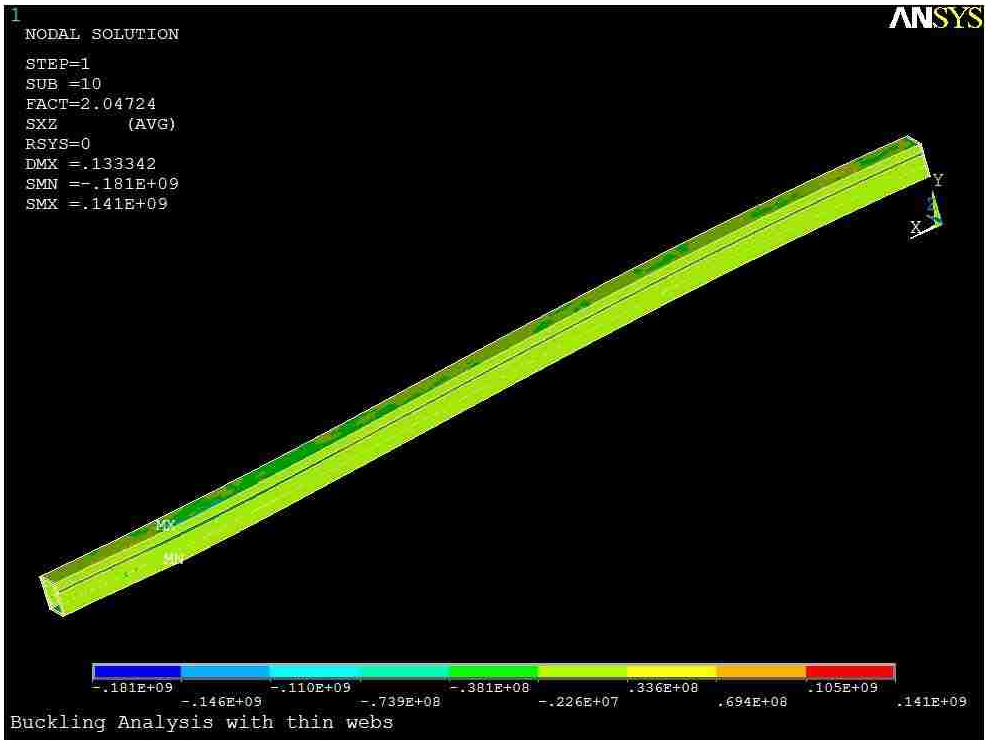

Figure 27: Shear stresses in xz-plane for thin webs

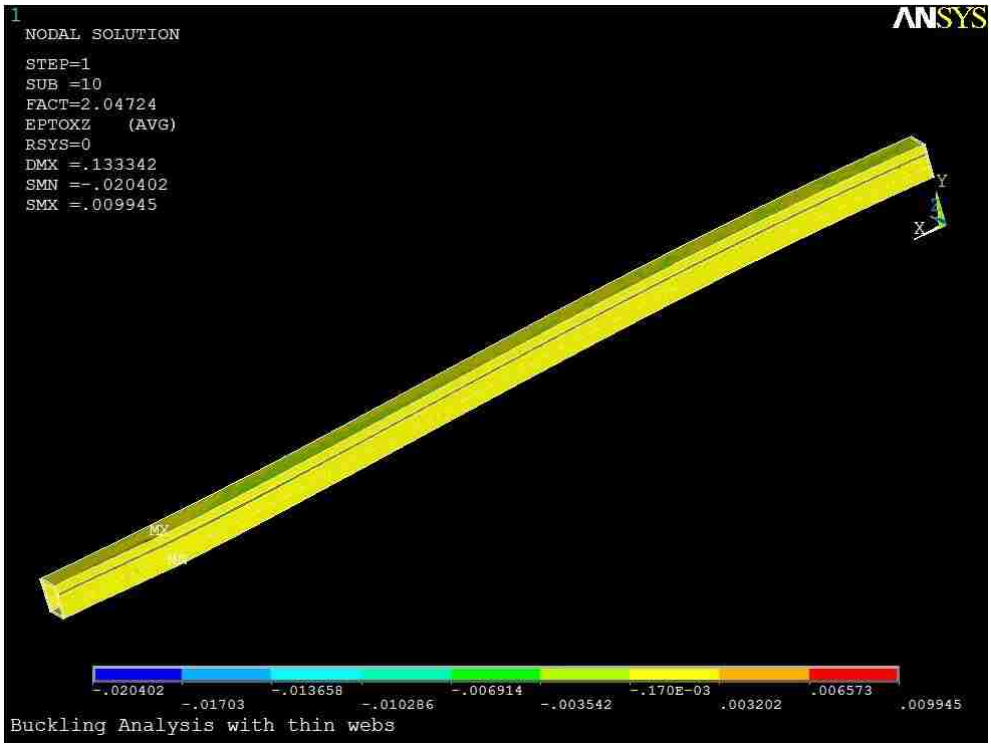

Figure 28: Strains in xz-plane for thin webs

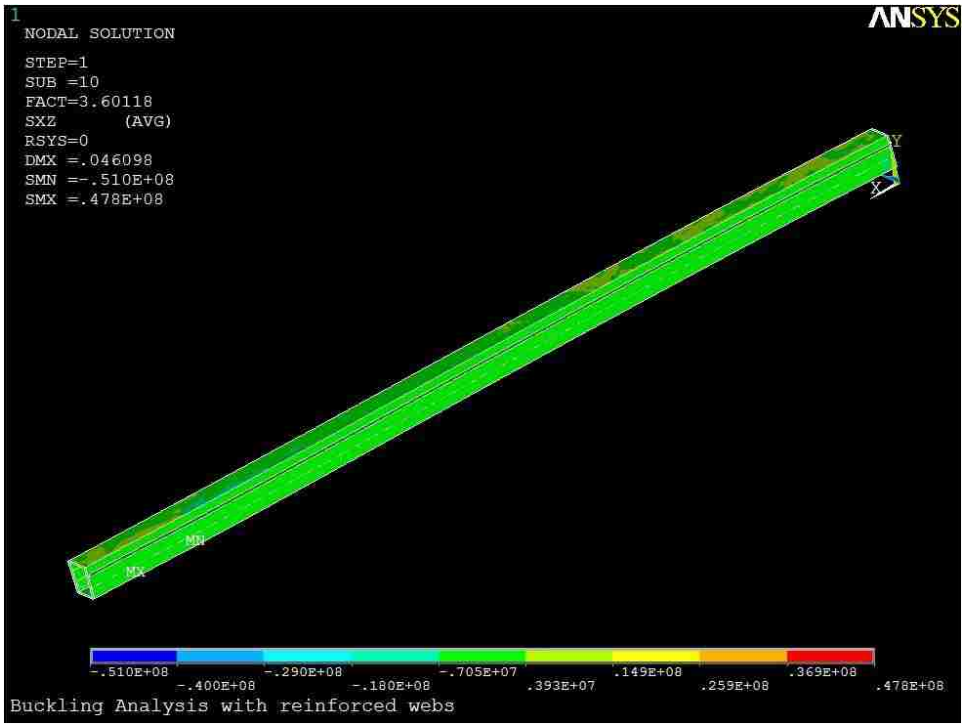

Figure 29: Shear stresses in xz-plane for reinforced webs

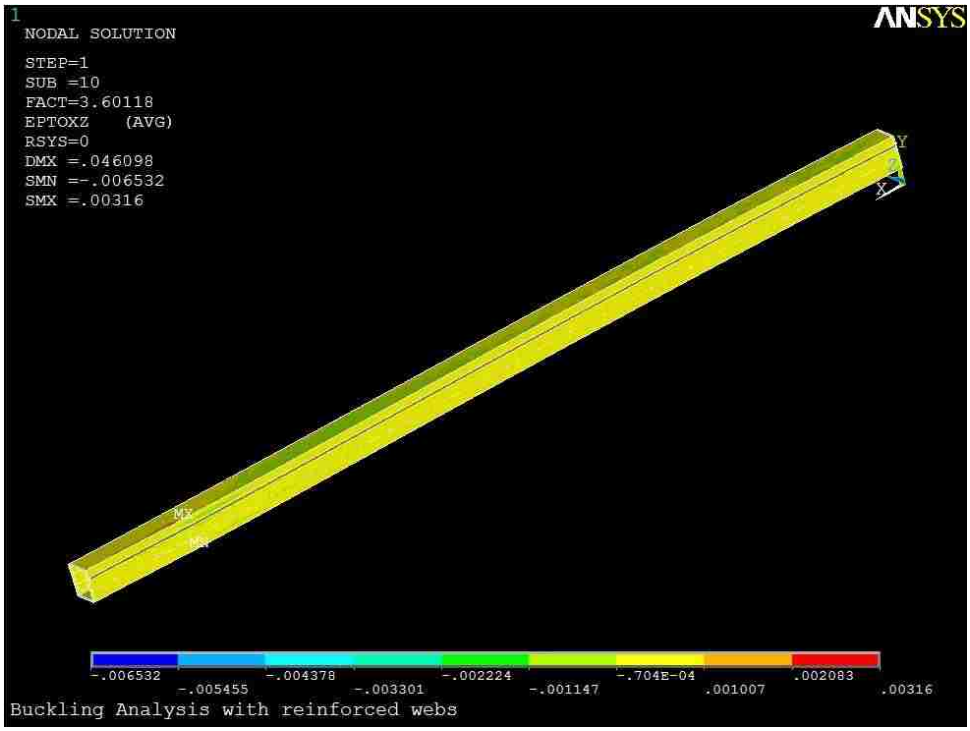

Figure 30: Strains in xz-plane for reinforced webs

8.4.1. Summary

Finite element analysis of composite structures is very difficult to solve realistically because imperfections, delamination and material degradations are not included in the analysis. A full scale blade test and computational analysis can be found in [12]. Two important conclusions may be drawn from buckling analysis.

a. Thickness of webs can be optimized to prevent spar failure in buckling.

b. The analysis only showed results of pre-buckling state. It is noted from literature and previous research that the structure may remain stable even after buckling deformation and continues to bear load. Although, stable post buckling time may be of very small order.

9. CONCLUSIONS

9.1. Summary

Following are the main results of the project:

a. Ideal load carrying capacity of a composite spar for wind turbine was calculated.

b. Test assembly capable of inducing bending loads on spar was fabricated in-house.

c. Multiple failure modes seen on spar after the experiment including possible buckling failure, debonding of shear webs, delamination of plies on compression flange, fracture and splitting of fibers along the spar and effects of stress concentration around rivet and pin holes.

d. spars with thin webs failed prematurely, POSSIBLY BY BUCKLING, which may have resulted due to high stresses in the webs.

e. Web reinforcement in spars may have increased buckling strength.

f. Although FEA may have provided global failure mechanism to certain accuracy, results are based on theoretical evaluations. Results with higher precision require detailed modeling and realistic conditions on model.

9.2. Recommended improvements for future work

a. Since fibers are hand laid, skilled work may improve results.

b. Webs may be reinforced further to avoid buckling failure completely but the thickness has to be optimized by reducing the weight of material in flanges. It is

generally known that carbon fiber reinforcements in the flange sections is a material of choice and may be used for greater stiffness and high strength to weight ratios.

c. More precise and detailed modeling of spar which includes but not limited to non-linearity effects, better ply drop terminations, delamination effects, properties of adhesive bond and epoxy, stiffness degradation and general imperfections of material may provide realistic results in computational analysis as well.

10. REFERENCES

1. Wind Energy Handbook. Structural Design. Gurit Holding AG. Switzerland
2. UpWind Design limits and sloutions for very large wind turbines. Riso National Laboratories. (2011)
3. Kyriakides, S., Arseculeratne, R., Perry, E.J. & Liechti, K.M. On the compressive failure of fiber reinforced composites. Int. J. Solid Structures, Vol. 32, No. 6/7, pp.689-738, Austin, TX. (1995)
4. Budainsky, B. & Fleck, N.A. Compressive failure of fiber composites. J. Mech. Phys. Solids, Vol.41, No.1, pp.183-211, Great Britain. (1993)
5. Liu, D., Fleck, N.A. & Sutcliffe, M.P.F. Compressive strength of fiber composites with random fiber waviness. J. Mech. Phys. Solids, Vol.52, pp.1482-1505, Cambridge. UK. (2004)
6. Mandell, J.F., Samborsky, D.D., Agastra, P. & Sears, A.T. Analysis of SNL/MSU/DOE Fatigue Database, Trends for Wind Turbine Blade Materials. SAND2010-7052, Albuquerque, NM. (2010)
7. Naik, N.K. & Kumar, R.S. Compressive strength of unidirectional composites: evaluation and comparison of prediction models. Dept. of Aerospace Engineering, IIT, Mumbia, India. (1999)
8. Griffin, D.A., Blade Systems Design Studies Volume I: Composite Technologies for Large Wind Turbine Blades. Sandia2002-1879, Albuquerque, NM, (2002)
9. Van Den Heuval, P.W.J., Van Der Bruggen, Y.J.W. & Peijs, T. Failure phenomenon in multi-fibre model composites: Part 1. An experimental investigation into the

influence of fiber spacing and fibre-matrix adhesion. Composites Part A 27A, pp.855-859, Elsevier Science Limited, Great Britain, (1996)

10. Ong, C.H. & Tsai, S.W. The Use of Carbon Fibers in Wind Turbine Blade Design. SAND2000-0478, Albuquerque, NM, (2000)
11. Hahn, H.T. & Williams, J.G. Compression Failure mechanisms in unidirectional composites. NASA Technical Memorandum 85834, Langley Research Center, Hampton, VA, (1984)
12. Jensen, F.M. Compression Strength of a Fibre Composite Main Spar in a Wind Turbine Blade. Riso-R-1393(EN), Riso National Laboratory, Roskilde, Denmark, (2003)
13. Ashwill, T.D. & Paquette, J.A. Composite Materials for Innovative Wind Turbine Blades. Sandia National Laboratories, Albuquerque, NM, (2007)
14. Ataabadi, A.K., Ziaei-Rad, S. & Hosseini-Toudeshky, H. Compression failure and fiber-kinking modelling of laminated composited. Dept. of Mechanical Engg. Isfahan University of Technology, Isfahan, Iran, (2011)
15. Ancona, D. & McVeigh, J. Wind Turbine – Materials and Manufacturing Fact Sheet. Office of Industrial Technologies, US DOE, (2001)
16. Banea, M.D. & Da Silva, F.M. Adhesively bonded joints in composite materials: An overview. Instituto de Engenharia Mecanica (IDMEC), Porto, Potugal, (2008)
17. Nairn, J.A., Harper, S.J. & Bascom, W.D. Effects of Fiber, Matrix and Interphase on Carbon Fiber Composite Compression Strength. Langley Research Center, NASA, Hampton, VA, (1994)

18. Sorenson, B.F., Jorgensen, E., Debel, C.P., Jensen, F.M., Jensen, H.M., Jacobsen, T.K. & Halling, K.M. Improved design of large wind turbine blade of fiber composites based on studies of scale effects (Phase 1). Riso-R-1390 (EN), Riso National Laboratory, Roskilde, Denmark, (2004)
19. Mandell, J.F., Reed, R.M., Samborsky, D.D. & Pan, Q. Fatigue Performance of Wind Turbine Blade Composite Materials. SED-Vol.14, Wind Energy ASME, (1993)
20. Wells, M., Schmidt, S., Barsotti, R., Vaughn, J. & Lackey, E. CRP Toughners for use in Composite systems. Composites & Polycon, American Composite Manufacturers Association, Tampa, FL, (2009)
21. Schubel, P.J. & Crossley, R.J. Wind Turbine Blade Design. Energies 5, pp.3425-3449, doi:10.3390/en5093425, Nottingham, UK, 2012
22. Probst, O., Martinez, J., Elizondo, J. & Monroy, O. Small Wind Turbine Technology. Wind Turbines, ISBN: 978-953-307-221-0, Rijeka, Croatia, (2011)
23. Wind Energy Handbook. Aerodynamics & Loads. Gurit Holding AG. Switzerland
24. EWEA Annual Report 2011
25. Energy Demands On Water Resources. Report to Congress on the Independency of Energy and Water. US Department of Energy, (2006)
26. Advantages and Disadvantages of Hydropower. Wind and Hydropower Technologies Program. US Department of Enegy, (2005)
27. DERAKANE® 8084 Epoxy Vinyl Ester Resin. Technical Data Sheet. ASHLAND, (2011)
28. EPOVIA® RF1001L-00 Unpromoted BPA-based Vinyl Ester Resin. Technical Data Sheet. ccp Composites. (2009-2013)

29. PRO-SET® ADV-176-QC. Material Safety Data Sheet. MSDS# ADV-176-QC-12a. Gougeon Brothers, Inc.

30. PRO-SET® ADV-276-QC. Material Safety Data Sheet. MSDS# ADV-276-QC-12a. Gougeon Brothers, Inc.

11. VITA

Syed Shahrukh Zafar, son of Syed Shamshad Zafar and Syeda Farhat Yasmin was born on January 7th, 1985 in Karachi, Pakistan. He attended Govt. Dehli College, Karachi from 2001 to 2003. In 2004 he entered NED University of Engineering & Technology, Karachi where he received the degree of Bachelors of Engineering in Mechanical Engineering in 2008. He started his professional career in March, 2008 as a Trainee Engineer in a Pakistan state owned Pak-Arab Refinery (PARCO) located in the province of Punjab. He was assigned a permanent role in 2010 as Maintenance Engineer. In June, 2011 he resigned from work and came to Lehigh University, PA for Masters of Science degree in Mechanical Engineering.

This manuscript was typed by Syed S. Zafar.